

1 **The histone methyltransferase NSD3 contributes to cohesin loading during** 2 **mitotic exit**

3
4 Grégory Eot-Houllier^{1,3*}, Laura Magnaghi-Jaulin^{1,2,3}, Gaëlle Bourguine¹, Erwan Watrin¹ and
5 Christian Jaulin^{1,2*}

6
7 ¹CNRS UMR 6290, University of Rennes1, IGDR (Institut de Génétique et Développement
8 de Rennes), 35043, Rennes cedex, France.

9 ²Present address: University of Rennes, EHESP, Inserm UMR 1085, Irset (Institut de
10 Recherche en Santé, Environnement et Travail), 35000, Rennes, France.

11 ³Equal contribution

12 *Corresponding authors

13 14 **Abstract**

15 During the cell cycle, dynamic post-translational modifications modulate the association
16 of the cohesin complex with chromatin. Phosphorylation / dephosphorylation and acetylation /
17 deacetylation of histones and of cohesin components ensure correct establishment of cohesion
18 during S phase and its proper dissolution during mitosis. In contrast, little is known about the
19 contribution of methylation to the regulation of sister chromatid cohesion. We performed a
20 RNA interference-mediated inactivation screen against 14 histone methyltransferases of the
21 SET domain family that highlighted NSD3 as a factor essential for sister chromatid cohesion in
22 mitosis. We established that NSD3 ensures proper level of the cohesin loader MAU2 and of
23 cohesin itself onto chromatin at mitotic exit. Consistent with its implication in the loading of
24 kollerin and cohesin complexes onto chromatin, we showed that NSD3 associates with
25 chromatin in early anaphase prior to that of MAU2 and RAD21 and dissociates from chromatin
26 upon cell's entry into prophase. Finally, we demonstrated that of the two NSD3 variant that
27 exist in somatic cells, the long form that carries the methyltransferase activity is the one that
28 acts in cohesion regulation. Taken together, these results describe a novel factor associated with
29 histone methylation in cohesin loading.

30

31

32

33

34

35 **Introduction**

36 To ensure faithful segregation of replicated DNA to daughter cells in mitosis, sister
37 chromatids are held together during replication and their cohesion must persist at centromeres
38 during the early stages of mitosis. Sister chromatid cohesion allows correct chromosome bi-
39 orientation towards spindle poles and establishment of tension between kinetochores. In human
40 somatic cells, sister chromatid cohesion is provided by a protein complex called cohesin
41 composed of the three core subunits SMC1A, SMC3, and RAD21, which form a ring that can
42 topologically embrace two chromatin fibres [1]. Cohesin core complex is further bound by
43 regulatory subunits, the Scc3 homologs SA-1 or SA-2, PDS5A or PDS5B and WAPL [2, 3].
44 Cohesin is loaded onto chromatin during exit from mitosis by the NIPBL/MAU2 complex, also
45 named Kollerin [4, 5]. NIPBL contains the cohesin loading activity, whereas MAU2 facilitates
46 NIPBL binding onto chromatin [6-9]. Establishment of sister chromatid cohesion occurs during
47 DNA replication when sister chromatids are synthesised [1]. From this stage onward until early
48 mitosis, Sororin binds to cohesin complex where it antagonizes WAPL anti-cohesive activity
49 [10]. Upon mitotic entry in vertebrate cells, the mitotic kinases CDK1, PLK1 and Aurora B
50 phosphorylate cohesin components and sororin, thereby rendering cohesin sensitive to WAPL
51 activity, which leads to the dissociation of cohesin molecules from the chromosome arms, in a
52 process known as the prophase pathway [11, 12]. During this process, sister chromatid cohesion
53 is protected from WAPL action at the centromere by the protein Shugoshin 1 (SGO1) and the
54 mitotic kinase Haspin. SGO1 competes with WAPL for cohesin ring association, and the SGO1
55 associated protein phosphatase 2A (PP2A) is believed to counterbalance the phosphorylation
56 of cohesin and Sororin [13, 14]. At the same time, Haspin binds to PDS5 and prevent interaction
57 with WAPL [15, 16]. Once all kinetochore are properly attached to microtubules at metaphase,
58 the spindle assembly checkpoint is turned off, which leads to the activation of the endoprotease
59 separase that cleaves cohesin subunit RAD21, thereby allowing opening of cohesin ring, its
60 dissociation from centromeric regions and segregation of the two sets of chromosomes [17].

61 The maintenance of sister chromatid cohesion at centromere until the metaphase-to-
62 anaphase transition is linked to a combination of several histone phosphorylations. They form
63 docking sites for effectors that counterbalance the cohesin dissociation induced by the prophase
64 pathway [18-22]. Despite its presence at centromeres, a role of histone methylation in protecting
65 centromere cohesion remains elusive [23]. Although Heterochromatin Protein 1 (HP1) favours
66 Haspin recruitment, and possibly that of SGO1 also, at centromeres, whether HP1 association
67 to H3K9me3 nucleosome is required for centromeric cohesion is still an open question [24-26].
68 Furthermore, preventing di-methylation of H3K4 at centromere by artificial acetylation through
69 HDAC3 depletion correlates with a premature separation of sister chromatids in early mitosis
70 [27]. However, the associated molecular mechanism remains to be established.

71 H3K4 methylation (mono-, di- and tri-methylation) is catalysed by protein macro-
72 complexes that belong to the SET domain methyltransferase family [28, 29]. These
73 methyltransferases are categorised into subfamilies that include the Nuclear receptor binding
74 SET Domain protein (NSD) subfamily, which comprises 3 members: NSD1, NSD2 (also
75 known as WHSC1, for Wolf-Hirschhorn Syndrome candidate 1) and NSD3 (WHSC1L1 for
76 WHSC1 protein Like 1). NSD methyltransferases act as oncoproteins in different types of
77 cancers [30, 31] and are specific to H3K36 [32-36]. However, NSD3 contribution to H3K36
78 methylation seems to be less efficient as compared to that of NSD2. Moreover, a contribution
79 to H3K4 di-methylation was shown following overexpression of the WHISTLE (WHSC1-like
80 1 isoform 9 with methyltransferase activity to lysine) isoform of NSD3 in NIH3T3 cells [32,
81 34, 36, 37]. In addition to their SET domain, NSD family members are characterised by the
82 presence of seven domains that bind to modified histones: five PHD domains (Plant Homeo
83 Domain) that recognize specific DNA sequences together with histone PTMs (methylated
84 Lysine or Arginine, acetylated Lysine), and two proline and tryptophan rich domains (PWWP)
85 which bind methylated lysines [37-39].

86 In somatic cells, NSD3 messenger RNA contains 24 exons and leads to the expression of
87 two protein isoforms called NSD3L and NSD3s [37, 38, 40] while a third isoform, called
88 WHISTLE, is specifically expressed in the testis from a downstream promoter [37]. The 1437
89 amino acid (aa) long form, NSD3L, includes the SET methyltransferase domain located in its
90 carboxy-terminus while the 647 aa short form, NSD3s, results from an alternative splice and
91 lacks the SET domain and, thus, the methyltransferase activity. NSD3s also differs from the
92 long form in its last 620-647 aa with only one PWWP domains that bind di-methylated on lysine
93 36 (H3K36me2) [41]. The one PWWP domain of NSD3s is required for the function of BRD4-
94 NSD3s-CHD8 complex in sustaining leukemia state, suggesting a combinatorial pathway
95 between H3K36me2 nucleosomes and acetylated nucleosomes bound by BRD4 to regulate
96 gene expression at concerned super-enhancers regions.

97 In the present work, we report the identification of NSD3 as a SET family member whose
98 inactivation resulted in precocious sister chromatid separation in early mitosis. We highlight
99 the requirement of NSD3 for interphase cohesion in post-replicative cells and show that NSD3
100 is involved in cohesin loading at mitotic exit. We also describe that NSD3 loads onto chromatin
101 in early anaphase prior to the association of the NIPBL/MAU2 cohesin loader complex with
102 chromatin. Finally, we demonstrate that the role of NSD3 in cohesin loading is mediated by the
103 NSD3L isoform that contains the SET methyltransferase domain.

104

105

106

107 **Results**

108 **NSD3 contributes to the maintenance of sister chromatids cohesion in mitosis**

109 We have previously reported that depletion of Histone DeAcetylase 3 (HDAC3) induces
110 precocious sister chromatid separation during mitosis prior anaphase onset. This effect is
111 accompanied by a forced acetylation of H3K4 and a loss of H3K4me2 at centromeres,
112 suggesting a contribution of centromeric H3K4me2 to sister chromatid cohesion in human.
113 Given that mutated histone versions cannot be specifically targeted to centromere and, further,
114 that H3K4 PTMs contribute to several chromatin-based processes beside centromere -in
115 particular gene regulation- pleiotropic effects resulting from the expression of a histone H3
116 version that can no longer be modified at the K4 residue are expected [42]. As an alternative,
117 we performed an RNAi-mediated inactivation screen for defective mitotic cohesion focussing
118 on 14 human SET domain-containing methyltransferases. In that aim, three different siRNAs
119 per SET methyltransferase were transfected in Kyoto HeLa cells, and mitotic chromosome
120 spreads were prepared and analysed for mitotic cohesion defects (Figure 1A). As shown in
121 Supplementary Figure 1, a single methyltransferase, NSD3, could be identified as leading to a
122 significantly increased proportion of prometaphase cells displaying separated sister chromatids
123 (Figure 1B-C, Figure S1). This screen therefore revealed NSD3 as a methyltransferase
124 important for sister chromatid cohesion in mitosis.

125 As NSD3 is involved in gene expression regulation, it remains possible that the cohesion
126 defects we observed could arise from the altered expression of cohesin components. To test this
127 possibility, we analysed total amounts of cohesin subunits and of cohesin loader MAU2 by
128 immunoblotting experiments of synchronised, RNAi treated cells. As shown in Supplementary
129 Figure 2, western blot analyses revealed that the expression levels of RAD21, SA1/SA2, SMC3
130 and of MAU2 were not altered following NSD3 depletion neither in nocodazole arrested-cells
131 nor after block release. Moreover, these immunoblotting experiments also indicated that global
132 di-methylation levels of H3K4 and H3K36 remained unaffected by NSD3 inactivation (Figure
133 S2), indicating that NSD3 involvement in sister chromatid cohesion is independent both of the
134 global disruption of H3K4 and H3K36 di-methylation status and of altered expression of
135 cohesin components and of MAU2.

136

137 **NSD3 is involved in cohesin loading regulation**

138 An increase in the proportion of mitotic cells exhibiting separated sister chromatids, such
139 as the one we observed upon NSD3 inactivation, can arise either from the accumulation of
140 prometaphase cells with defective mitotic cohesion or from a premature entry of cells into
141 anaphase. In order to discriminate between these two possibilities, we first investigated the
142 status of the spindle assembly checkpoint activity by analysing both the presence of the mitotic

143 checkpoint complex kinase BUB1 and of the centromeric cohesin protector SGO1 at
144 pericentromeric regions by indirect immunofluorescence experiments. As shown in Figure 2,
145 BUB1 kinase could be detected at kinetochores of cells displaying defective cohesion,
146 indicating that the spindle checkpoint is still active and that, therefore, cells are arrested in
147 prometaphase (Figure 2A). Similarly, SGO1 could be detected at centromeres of separated
148 sister chromatids following NSD3 depletion, confirming that these cells were indeed blocked
149 in prometaphase (Figure 2B) instead of having entered anaphase. Altogether these observations
150 indicate that NSD3 is required for a proper sister chromatid cohesion in mitosis and suggests
151 that this role does not depend on SGO1-mediated protection of centromeric cohesin.

152 Thus, we next aimed at determining whether defective cohesion detected in mitotic cells
153 after NSD3 depletion was already present in interphase post-replicative cells. In that goal, we
154 analysed cohesion between sister chromatids in interphase cells by DNA Fluorescent *In Situ*
155 Hybridization (FISH) using probes that bind to chromosome 11 centromere regions in cells
156 synchronised in G2-phase (Figure 2C-E). Cohesion status was assessed by measuring distances
157 between paired FISH signals in control cells and in cells depleted for NSD3 as well as cells
158 depleted for RAD21 used as a positive control of defective cohesin. In control cells, mean
159 distance between paired dots was 0.52 μ m and increased to 0.68 μ m in RAD21-depleted cells
160 and to 0.67 μ m upon NSD3 depletion. These experiments revealed that NSD3 depletion
161 resulted in defective sister chromatid cohesion in G2 cells, indicating that NSD3 contributes to
162 cohesion before cells enter mitosis, i.e. in interphase.

163 Then, we asked whether NSD3 could be involved in the loading of cohesin and/or of
164 kollerin onto chromatin, a process that takes place at mitotic exit. In that aim, control and NSD3-
165 depleted cells were synchronised by single thymidine arrest-and-release coupled to mitotic
166 arrest using the mitotic spindle poison nocodazole (Figure 3A). Cells were harvested at different
167 time points after release from the mitotic arrest and fractionated into soluble and chromatin
168 fractions that were analysed by immunoblotting experiments after SDS-PAGE. As shown in
169 Figure 3B, NSD3 inactivation did not impact on cell's mitotic exit as both condensin II complex
170 subunit HCAP-D2 unloading and histone H3 Serine10 de-phosphorylation occurred with
171 identical kinetics between control and NSD3 inactivated cells. However, accumulation of
172 cohesin subunits on chromatin over time was reduced by around 50 % in NSD3-depleted cells
173 when compared to that in control cells. Remarkably, similar albeit more modest 30 % reduction
174 was also observed for the kollerin subunit MAU2. This reduction in detected protein signals
175 was not due to reduced amounts of chromatin as both chromatin associated enzyme
176 topoisomerase II and histones were present at similar levels in control and NSD3-depleted cells.

177 This experiment showed that NSD3 inactivation leads to reduced amounts of cohesin and
178 MAU2 loaded onto chromatin during exit from mitosis, indicating that NSD3 contributes to the
179 loading of both cohesin and kollerin complexes at the end of mitosis.

180 **NSD3 is released from chromatin at mitosis onset and reloaded in early anaphase**

181 As shown in Figure 3, immunoblotting analysis of chromatin fractions revealed that both
182 NSD3 long and short variants were absent from chromatin in mitosis-arrested control cells and
183 progressively accumulated upon release and progression to G1 phase.

184 To characterise this dynamic behaviour in more details, we aimed at analysing the
185 localization of NSD3 at the different stages of the cell cycle by indirect immunofluorescence
186 experiments. First, NSD3 antibody staining specificity was determined by RNAi-mediated
187 inactivation of NSD3 followed by antibody staining that resulted in a strong reduction of the
188 NSD3 antibody fluorescence signal down to background signal (Supplementary Figure 3).

189 Next, we performed NSD3 antibody staining in an asynchronous HeLa cell population
190 and monitored corresponding signals in interphase cells and in mitotic cells using both
191 chromosome morphology and H3S10 phosphorylation mark staining as a mean to identify the
192 different stages of mitosis. These immunostaining experiments were performed with and
193 without detergent-based pre-extraction of the soluble pool of proteins (Figure 4A-B).
194 Fluorescence microscopy imaging of these samples revealed that NSD3 signal is associated
195 with chromatin in interphase and prophase cells and is essentially absent from chromosomes
196 from early prometaphase until metaphase (Figure 4B). A very weak NSD3 signal could still be
197 detected on chromatin in prometaphase cells after pre-extraction. To test if that remaining signal
198 is due to the presence of a fraction of NSD3 on chromatin, we looked for the presence of NSD3
199 on chromosome spreads. As shown in Figure 4C, the weak labelling observed in control siRNA
200 treated prometaphase cells did not co-localize neither with whole chromosomes nor with
201 centromere regions as revealed by CREST serum co-staining. No obvious difference was
202 observed when mock-siRNA treated prometaphase cells were compared to NSD3-siRNA
203 treated prometaphase cells (Figure 4C) indicating that the weak fluorescence signal observed
204 on pre-extracted prometaphase cells (Figure 4B) represents non-specific background. After the
205 metaphase-to-anaphase transition, NSD3 signal is detected on chromatin as soon as in early
206 anaphase (Figure 4B). These results were confirmed using two doxycycline-inducible cell lines
207 we established and that allow specific expression of the long or the short isoforms of NSD3
208 fused to a LAP (Localization and affinity purification) tag containing in particular an Emerald
209 GFP (Figure S4 and next section), altogether indicating that NSD3 isoforms both associate with
210 chromatin in interphase and early prophase, dissociate from chromosomes in prophase and re-
211 associate with chromosome at anaphase, similar to the dynamic behaviour of cohesin and
212 kollerin complexes.

213 Finally, we repeated these fluorescence microscopy experiments in the two LAP-NSD3
214 cell lines to assess differential chromatin association/dissociation of NSD3 relative to that of
215 cohesin and of kollerin (Figure 4D-E, Figure S5). These experiments showed that association
216 with chromatin of LAP-NSD3L occurs prior to that of RAD21 and of MAU2 (Figure 4D-E,

217 Figure S5) and in an identical fashion for LAP-NSD3s (not shown). Thus, NSD3 is removed
218 from chromatin after mitosis entry and is reloaded back at early anaphase shortly before the
219 recruitment of kollerin and of cohesin.

220

221 **Sister chromatid cohesion depends on the long form of NSD3**

222 Our work has revealed that RNAi-mediated inactivation of NSD3 resulted in cohesin and
223 kollerin loading and in subsequent cohesion defects both in interphase and in mitotic cells. As
224 the siRNA we used targeted both long and short isoforms of NSD3 protein, we aimed at
225 determining whether one or both isoforms were involved in cohesion regulation. In that goal,
226 we designed isoform-specific siRNAs (two per isoforms) that selectively depleted each of them
227 in an efficient manner as revealed by immunoblotting experiments (Figure 5A). We then
228 compared the ability of these isoform-specific siRNAs to induce precocious sister cohesion
229 defects in mitotic cells as compared to that of siRNAs targeting both of them. As shown in
230 Figure 5B, both siRNAs targeting the long form of NDS3 resulted in defective mitotic cohesion,
231 while the siRNAs targeting the short form did not have any effect on cohesion despite an
232 efficient protein amount reduction. This result indicates that the long form of NSD3, and not its
233 short version, is involved in sister chromatid cohesion.

234 To confirm this result, we made use of the cell line we established (see above and Figure
235 5C-D) that expresses a LAP-tagged version of NSD3L that has been rendered resistant to NSD3
236 RNAi (see Methods for details) and we assessed its ability to rescue defective mitotic cohesion
237 upon depletion of NSD3L&s and NSD3L using specific siRNAs. Treated cells were analysed
238 by scoring the percentage of prometaphase cells exhibiting precocious sister chromatid
239 separation in each condition with and without doxycycline induction (Figure 5D-E). The cell
240 line heterogeneity in expressing LAP-NSD3L allowed us to use GFP-negative cells as an
241 internal control (Figure 5C). In the absence of doxycycline, we confirmed that depleting either
242 both NSD3 isoforms or NSD3L only resulted in premature sister chromatid separation, identical
243 to the situation in doxycycline-treated cells that were negative for GFP signals (Figure 5E, black
244 and grey bars, respectively). By contrast, in cells where LAP-NSD3L was expressed (GFP
245 positive cells), the proportion of mitosis displaying precocious sister chromatid separation was
246 significantly reduced (Figure 5E, green bars), which indicated that ectopic correction of NSD3L
247 protein amount was able to rescue defective mitotic cohesion, thereby establishing NSD3L as
248 the isoform required for proper sister chromatid cohesion.

249

250 **Discussion**

251 Sister chromatid cohesion is established during S phase, depends on cohesin which
252 loading onto chromatin requires the kollerin complex and stands essential for proper

253 chromosome segregation at anaphase. Here, we show that NSD3 is required for the recruitment
254 of the cohesin loader MAU2 and, consequently, to that of cohesin to chromatin at mitosis exit.
255 Therefore, we propose that precocious sister chromatid separation observed in mitotic cells
256 upon NSD3 inactivation is an indirect consequence of defective kollerin recruitment and, as a
257 consequence, of cohesin loading onto chromatin. In full agreement with its function in
258 promoting Kollerin targeting on chromatin, our observation showed that the dynamic
259 localisation behaviour of NSD3 is similar to that of MAU2 and of cohesin [5]. We also noticed
260 that NSD3 binds to chromatin during anaphase shortly before MAU2 and RAD21. Therefore,
261 NSD3 is unlikely to interact with NIPBL/MAU2 prior to their targeting to the chromatin.
262 Rather, NSD3 may promote kollerin loading onto chromatin by facilitating its binding at the
263 end of mitosis. Consistent with this possibility, yeast MAU2 homologue Scc4 is necessary to
264 load Scc2 onto chromatin *in vivo*, but has no affinity to bind DNA, implying the requirement
265 for a protein receptor [6-8]. NSD3 represents a good candidate to play such a role as receptor,
266 thereby triggering the recruitment of NIPBL/MAU2 complex via direct protein-protein
267 interaction. Indeed, recent reports have shown that NSD3 interacts with the transcriptional
268 regulator BRD4, which in turn interacts with NIPBL through its extra-terminal domain and
269 stabilizes it on specific chromatin regions in vertebrate cells [43, 44]. It is thus tempting to
270 propose that BRD4/NSD3 acts as a platform that binds and loads NIPBL/MAU2 onto
271 chromatin.

272 Alternatively, the contribution of NSD3 could be to render chromatin regions amenable
273 for Kollerin loading via chromatin remodelling. Consistent with this view, it has been reported
274 that NSD3 acts as an adaptor protein bridging the BET domain of BRD4 and the chromatin
275 remodelling factor CHD8. Moreover, two reports from Franck Uhlmann's laboratory have
276 demonstrated that the chromatin remodeler RSC (Remodels the Structure of Chromatin) acts as
277 a chromatin receptor by interacting physically with the Scc2/Sc4 complex in the yeast *S.pombe*
278 [45-47]. They have also shown that RSC plays also a conserved role by promoting nucleosome
279 removal in order to render the DNA naked for the binding of the cohesin complex independently
280 of Scc2/Sc4 [46, 47]. Thus, one can imagine that similarly to the yeast process,
281 BRD4/NSD3/CHD8 complex acts in human kollerin recruitment through two complementary
282 mechanisms. Firstly, CHD8 nucleosome sliding activity displace nucleosomes to create a
283 nucleosome free region. Secondly, BRD4 ensures the physical interaction with the Kollerin
284 complex [48]. In this context, as proposed by Shen & al [44], NSD3 bridge BRD4 and CHD8
285 and thus would generate an integrated molecular process of kollerin recruitment onto
286 chromatin. Similarly, additional chromatin remodellers have been described to contribute to
287 cohesin loading [49, 50]. Whether NSD3 requirement for Kollerin loading onto chromatin
288 involves chromatin remodelling will require dedicated investigations.

289 In addition, our results revealed that MAU2 and cohesin loading onto chromatin involves
290 only the long form of NSD3. Domains interacting with BRD4 and CHD8 are common for both

291 NSD3 isoforms [44]. Therefore, if physical interaction with these two partners would be
292 sufficient for the NSD3 regulation of cohesin loading, one could have expected that only
293 depletion of both isoforms would prevent cohesin loading. In contrast to this possibility, we
294 showed that only the depletion of NSD3L and not that of NSD3s, resulted in defective cohesion.
295 This implies that, in addition to its possible association with BRD4 and CHD8, NSD3L function
296 in kollerin loading requires further properties, such as additional co-factors or enzymatic
297 activity. In accordance with the latter hypothesis, NSD3L is the one NSD3 isoform that contains
298 the methyltransferase activity. It is thus tempting to propose that NSD3L acts by generating
299 post-translational modifications of yet unidentified substrates. In our current state of
300 knowledge, H3K36me2 represents the best candidate for further investigations concerning the
301 contribution of NSD3 to the recruitment of cohesin loaders and cohesin onto chromatin. Indeed,
302 H3K36me2 is found in active gene promoters and NIPBL was also enriched to those region in
303 human cells [51-53]. One can speculate that NSD3L would act to render chromatin prone for
304 further kollerin targeting by methylating histones. The use of a mark that is stable throughout
305 mitosis, as H3K36me2, could be essential for the epigenetic inheritance of cohesin loading
306 sites.

307

308 **Materials and methods**

309 **Antibodies.**

310 Antibodies dilutions for western blotting (WB) and immunofluorescence (IF) are indicated
311 below. The antibodies used were: rabbit anti-NSD3 (Proteintech 11345-1-AP) WB: 1/1000, IF:
312 1/1000 ; mouse anti-RAD21 (Millipore ref 05-908) WB:1/5000, IF: 1/1000 ; rabbit anti-MAU2
313 (Abcam Ab183033) WB: 1/5000, IF: 1/1000 ; mouse anti-SA2 (Santa Cruz sc-81852)
314 WB:1/500 ; rabbit anti-SMC3 WB: 1/1000 [54], rabbit anti-hCAP-D2 1/1000 [55], mouse anti-
315 Topoisomerase II α (Ki-S1) Millipore (MAB4197) WB: 1/2000 ; mouse anti-p-H3S10
316 (Millipore 05-806) WB: 1/10 000, IF: 1/20 000, rabbit anti-H3K4me2 (C64G9) (Cell Signaling
317 Technology #9725) WB: 1/5000 ; rabbit anti-H3K36me2 (Active Motif 39056) WB: 1/5000 ;
318 mouse anti-H4 (Abcam Ab31830) WB: 1/2000 ; rabbit polyclonal anti-actin (Sigma A5060)
319 WB: 1/10 000; mouse anti- α -tubulin (Sigma T5168) WB: 1/5000 ; mouse monoclonal anti-
320 Bub-1 (Sigma B0561) IF: 1/100 ; mouse anti-GFP (Roche 11814460001) WB: 1/500, IF: 1/500.
321 Rabbit anti-Sgo1 antibody was a gift from Prof. Yoshinori Watanabe (Japan) IF: 1/1000 [56];
322 Human CREST serum was a gift from Dr Isabelle Bahon-Riedinger (France) IF: 1/4000.
323 Horseradish peroxidase coupled secondary antibodies (Jackson Immunoresearch) (WB: Mouse
324 1/5000 Rabbit 1/25000) and Alexa Fluor-coupled secondary antibodies from Invitrogen (IF:
325 1/1000) were used for WB and IF detection, respectively.

326

327 **Plasmid construction and cell line generation.**

328 A fragment containing an inducible TRE tight promoter and a LAP tag (Flag tag followed by
329 emerald Green Fluorescent Protein tag) was inserted at the XhoI site of the pBSKDB-CAG-
330 rtTA2sM2-IRES-tSkid-IRES-Neo plasmid (Addgene #62346), generating a vector named
331 pGEH_ind_LAP-C. In this vector, NSD3s or NSD3L were cloned in frame in C-terminal of the
332 LAP tag after PCR amplification from plasmids pMSCV_MigR1_NSD3short and
333 pMSCV_MigR1_NSD3long, kindly given by CR.Vakoc [44]. All PCR were realized with the
334 Q5 high fidelity polymerase (NEB M0493S) and all constructions and intermediates were
335 generated by NEBuilder HiFi DNA assembly cloning kit according to manufacturer
336 recommendations (NEB E5520S). Plasmids and their maps will be provided upon request.

337 For generation of HeLa-LAP-NSD3L and HeLa-LAP-NSD3s cell lines, 5 µg of corresponding
338 plasmids, supplemented with 10 µl of P3000 in 125 µl Opti-MEM (ThermoFischer Scientific
339 31985062), were mixed with 7.5 µl lipofectamine 3000 in 125 µl Opti-MEM. After 5 min
340 incubation at room temperature, mix containing plasmids were transfected in HeLa-Kyoto
341 seeded the day before in 2.25 ml of complete medium in 6 well plates. 24h later, cells were
342 trypsinized and 1/10 or 1/50 of the cells was seeded in a 150 mm culture dish in 25 ml of
343 complete medium containing 1 mg/ml of G418 (ThermoFischer Scientific 11811023). Selection
344 lasted for 2-3 weeks with replacement of the antibiotics supplemented medium each 2-3 days.
345 Then, cells were induced for LAP-NSD3 expression with 2µg/ml of doxycycline (Merck D9891-
346 1G) for 48h and GFP positive cells were FACS sorted using the CytomeTRI platform (Biosit
347 SFR UMS CNRS 3480 – INSERM 018 - Rennes) and cultured for another 2 weeks under
348 selection pressure, but without induction. Then, cells lines were subcloned by limiting dilution
349 in 96 well plate and after 2 weeks of selection, around 30 clones were tested for LAP-NSD3
350 expression for each NSD3 variant. Despite all this process, no homogeneous clonal cell line
351 could be obtained. For the LAP-NSD3s construct, we always obtained clones that expressed
352 the fused protein constitutively. By contrast, expression of LAP-NSD3L in the selected cell
353 lines was inducible as expected.

354

355 **Cell culture and treatment**

356 All experiments presented in this paper were performed with HeLa-Kyoto cells or cell lines
357 constructed from these cells. All cell lines were cultured in Dulbecco's Modified Eagle's
358 Medium with glutamine analogue Glutamax (Thermofischer Scientific 31966047),
359 supplemented with 10% fetal bovine serum and a cocktail of penicillin/streptomycin antibiotics
360 (Thermoficher Scientific 15140-122) at 100U/ml and 100µg/ml final concentration,
361 respectively. Stable cell lines were maintained in culture with G418 (1mg/ml). Doxycycline
362 was used at 1 µg/ml in medium to induce expression of the exogenous tagged protein and was
363 replaced with fresh doxycycline-containing medium after 48h when it was necessary. To
364 synchronize cells, thymidine (Merck T1895-1G) was added to the medium 8 hours post-

365 transfection at a final concentration of 2 mM and cells were cultured for 24h, followed by two
366 successive 3 min PBS washes and incubation with complete medium supplemented with 100
367 ng/ml nocodazole (Merck M1404) for another 16h to arrest cells in prometaphase. Then, cells
368 were harvested by mitotic shake-off, washed as described for the previous release and seeded
369 in fresh complete medium in new plates. All medium were pre-warmed at 37°C before using in
370 synchronisation experiments.

371

372 **siRNA transfection**

373 HeLa cells were transfected with 20 nM siRNA for 72h, unless otherwise stated in the figure
374 legends, with Hiperfect (Qiagen) following manufacturer recommendations. As a general
375 guideline, for a 6 well transfection, 10 µl of Hiperfect reagent and 2,5µl of 20 µM stock siRNA
376 were mixed in 87,5 µl of Opti-MEM and added to 300 000 HeLa cells seeded in suspension in
377 2,4 ml of complete medium. Medium was replaced after 48h transfection and cells were
378 trypsinized and diluted if necessary. siRNA used in the experiments were described below and
379 were purchased from Qiagen of Dharmacon. Those used for the methyltransferase screening
380 can be communicated upon request.

siRNA name	Gene targeted	Sequence sense	Sequence antisense
NSD3-a	NSD3	CGAGAGUAUAAAGGUCAUAdTdT	UAUGACCUUUUAUCUCUCGdTdA
NSD3-b	NSD3	GACCAAGAUCUGUGCUGAAAdTdT	UUCAGCACAGAUCUUGGUCdGdT
NSD3-c	NSD3	AAUGGGUAUCCAUCAUCAAdTdT	UUGAUGAUGGAUACCCAUUdTdG
NSD3L-A	NSD3L-3'UTR	GGUCUUAAUUGGAGAGAAUdTdT	AUUCUCUCCAAUUAAGACcAdG
NSD3L-B	NSD3L-3'UTR	GGGACAGGCUAUUGGACAAAdTdT	UUGUCCAAUAGCCUGUCCcAdT
NSD3s-a	NSD3s-3'UTR	GGUUUGAGCUGGAUGGGUAdTdT	UACCCAUCCAGCUCAAACcGdA
NSD3s-b	NSD3s-3'UTR	UCAGAAACUCAUCGGAAAUdTdT	AUUUCCGAUGAGUUUCUGAdAdA
Luc	Luciferase	CGUACGCGGAAUACUUCGAdTdT	UCGAAGUAUCCGCGUACGdTdT
Rad21	Rad21	CGAUGAGCCCAUUAUUGAAAdTdT	UUCAUAAUGGGCUCAUCGdTdT

381

382 **Chromosome spreads**

383 Cells harvested from a 6 well plate were subjected to hypotonic shock in 4.5 ml of 75 mM KCl
384 for 15 min at room temperature and 500 µl of Carnoy's fixative (3 vol methanol/1 vol acetic
385 acid) was added. Cells were centrifuged at 250g and the pellet was resuspended in 5 ml of
386 Carnoy's fixative. This operation was repeated 3 more times and the pellet were keep at -20°C
387 in 300 µl of Carnoy's fixative overnight. Then, we dropped 30 µl of cells on a dry slide, let
388 them dry for 2h at room temperature, and incubate slides for 5 min in fresh 5% GIEMSA (Merck
389 1.09203) solution diluted in 100 ml Gurr buffer (ThermoFisher scientific 10582-013).

390 Following 3-5 washes in distilled water, giemsa stained cells were mounted with entellan.
391 Alternatively, for immunofluorescence on chromosome spreads, following hypotonic shock
392 around 50 000 swollen cells in 200µl of KCl 75mM were cytopun on a slide for 5 minutes at
393 900 rpm (Cytospin 4; Thermo Scientific) and were fixed in 3% paraformaldehyde/PBS for
394 further immuno-labelling.

395

396 **Immunofluorescence**

397 When stated, soluble contents of cells were pre-extracted by incubation for 1 min in 0,1% Triton
398 (Merck T8787-50ML) diluted in PBS 1X (ThermoFisher Scientific 10010-015). Otherwise,
399 cells were fixed 10 min in 4% Paraformaldehyde (EMS 15710) diluted in PBS 1X pH 7.2-
400 pH7.4 final. Slides or coverslips were then washed three times 5 min in PBS 1X, permeabilized
401 with 0.1% Triton X-100 for 10 min, washed three times in PBS 1X and blocked by incubation
402 with 5% FCS in PBS 1X for 1h min at room temperature. This last solution was used to dilute
403 primary and secondary antibodies. Slides or coverslips were then incubated overnight at 4°C
404 with primary antibodies, washed three times with PBS 1X and then incubated for 1 hour at
405 room temperature with fluorochrome-conjugated secondary antibodies. The DNA was stained
406 with DAPI (100 ng/ml in PBS) and slides were mounted in Prolong-Gold medium
407 (ThermoFisher Scientific P36982).

408

409 **Microscopy and image analysis**

410 Images were acquired with an epifluorescence microscope (Zeiss AxioImager.M2) equipped
411 with Zeiss “Plan-Apochromat” 40x/1.3 and 63x/1,40 oil objectives, a Coolsnap HQ² CCD
412 camera (Photometrics) and Zeiss Axiovision software (version 4.2). Signals were quantified
413 with ImageJ software (Rasband, W.S., ImageJ, US National Institutes of Health, Bethesda,
414 Maryland, USA, <http://rsb.info.nih.gov/ij/>, 1997-2005).

415

416 **Fluorescent In Situ Hybridization**

417 DNA FISH was performed as previously described [57], with the exception that cells were fixed
418 with Carnoy’s fixative as described above and processed for FISH after spreading on glass
419 slides. Only pairs for which the dots could be clearly resolved were considered in the analysis.
420 The probe used for FISH targets the alpha-satellite sequence AgGgTtTcAgAgCtGcTc that is
421 specific of the centromeric region of the 11 chromosome. In the probe sequence, uppercases
422 correspond to DNA whereas lowercases correspond to a locked nucleic acid, which is a
423 modified RNA nucleotide in which the ribose moiety is modified with an extra bridge
424 connecting the 2’ oxygen and 4’ carbon. The probe was coupled with an Alexa-488 fluorophore.

425

426 **Cell extracts and western blotting**

427 For whole cell extracts, proteins were extracted by directly resuspending cells pellet in Laemmli
428 buffer (60 mM Tris-HCl pH6.8, 10% glycerol, 2% SDS, 0.05% bromophenol blue, 5% β -
429 mercaptoethanol). When fractionation was required, cells were collected by trypsinization and
430 washed once with ice-cold PBS. The final cell pellet was resuspended in extraction buffer
431 (20 mM Tris pH 7.5, 100 mM sodium chloride, 5 mM magnesium chloride, 0.2% NP-40, 10%
432 glycerol, 0.5 mM dithiothreitol) supplemented with EDTA-free tablets of protease inhibitors
433 (Merck 5892953001) and home-made phosphatase inhibitors cocktail (5 mM sodium fluoride,
434 10 mM β -glycerophosphate, 1 mM sodium pyrophosphate and 0.2 mM sodium orthovanadate
435 final concentration respectively). Cells were lysed on ice by ten passages through a 27-gauge
436 needle. Lysates were incubated for 10 minutes on ice and were then centrifuged (12 000 g,
437 5 minutes, 4°C) for collection of the soluble protein extract. The chromatin-containing pellet
438 was washed four times with extraction buffer (12,000 g, 5 minutes, 4°C) and then directly
439 resuspended in Laemmli buffer.

440 For immunoblotting, lysed cells were heated for 5 minutes at 95°C. Samples were then
441 subjected to SDS-PAGE in a 4-20% polyacrylamide gradient gel (Biorad #4561094) and
442 transferred to ready-to-use PVDF membranes (Biorad #1704156) with a Trans-Blot Turbo
443 transfer system (Biorad). Following saturation for 1h hour in PBS 1X containing 5% milk and
444 0.1% tween-20, membranes were incubated overnight at 4°C with primary antibodies and then
445 for 1 hour at room temperature with horseradish peroxidase (HRP)-conjugated secondary
446 antibodies, according to standard procedures. For NSD3 western blotting, saturation and
447 incubation were performed with similar procedures, except that saturation and incubation buffer
448 was supplemented with 10% milk instead of 5% and 150 mM NaCl. For revelation, membranes
449 were treated with the substrate HRP Immobilon ECL kit (Merck WBKLS0500) and signal was
450 detected with an Amersham Imager 680 (GE Healthcare) or with Amersham hyperfilm ECL
451 (Merck GE28-9068-35). Quantification of band signal intensity were realized with the
452 Analyze/Gels tools of ImageJ.

453

454 **Statistics**

455 All statistical analysis were performed with GraphPad Prism v6.05 (GraphPad Software). For
456 the comparison of PSCS or mitotic index between NSD3 depleted cell lines, we performed one-
457 way analysis of variance (ANOVA) followed by Dunett *post hoc* analysis, assuming normal
458 law for the repartition of the means. Comparisons of fluorescence intensity from a
459 representative experiment were analysed in nonparametric Kruskal Wallis test followed by
460 Dunn's multiple comparison correction. For the comparison of distance in FISH experiment,
461 one-way ANOVA was used followed by Bonferroni's multiple comparisons test. For all
462 statistical tests, an alpha risk of 0.05 was used.

463 **Author contributions**

464 G.E.-H and L.M.-J designed and performed the experiments. G.B contributed to plasmid
465 constructions. G.E-H, L.M-J and E.W analysed data. G.E-H and E.W wrote the manuscript.
466 C.J. designed and supervised the project, provided funding and revised the manuscript.

467

468 **Competing interests**

469 The authors have no conflict of interest to declare.

470

471 **Acknowledgments**

472 We would like to especially thank Dr. Rozenn Gallais for her singular contribution to this study.
473 We would like to thank Prof. Christopher Vakoc (Cold Spring Harbor Laboratory, USA), Dr.
474 Christophe Escudé (National Museum of natural history, France), Prof. Yoshinori Watanabe
475 (University of Tokyo, Japan), Prof. and Dr Isabelle Bahon-Riedinger (Rennes University
476 Hospital, France) for providing reagents. We also thank Laurent Deleurme from the Flow-
477 cytometry platform CytomeTRI of the BIOSIT SFR UMS CNRS 3480 – INSERM 018 unit,
478 for the FACS cell sorting of LAP-NSD3 HeLa cells lines. G.E.-H, L.M.-J, G.B and E.W are
479 investigators at the CNRS. C.J. is investigator at INSERM. This work was funded by the French
480 National Research Agency (ANR, project "EpiCentr"), the *Région Bretagne* (SAD grant), *the*
481 *Cancéropôle Grand Ouest*, *the Ligue Contre le Cancer (Comité Grand Ouest)* and *the*
482 *Fondation ARC pour la Recherche sur le Cancer*.

483

484 **References**

- 485 1. Nasmyth, K., and Haering, C.H. (2009). Cohesin: its roles and mechanisms. *Annu Rev Genet*
486 *43*, 525-558.
- 487 2. Makrantonis, V., and Marston, A.L. (2018). Cohesin and chromosome segregation. *Curr Biol*
488 *28*, R688-R693.
- 489 3. Nishiyama, T. (2019). Cohesion and cohesin-dependent chromatin organization. *Curr Opin*
490 *Cell Biol* *58*, 8-14.
- 491 4. Ciosk, R., Shirayama, M., Shevchenko, A., Tanaka, T., Toth, A., Shevchenko, A., and Nasmyth,
492 K. (2000). Cohesin's binding to chromosomes depends on a separate complex consisting of
493 Scc2 and Scc4 proteins. *Mol Cell* *5*, 243-254.
- 494 5. Watrin, E., Schleiffer, A., Tanaka, K., Eisenhaber, F., Nasmyth, K., and Peters, J.M. (2006).
495 Human Scc4 is required for cohesin binding to chromatin, sister-chromatid cohesion, and
496 mitotic progression. *Curr Biol* *16*, 863-874.
- 497 6. Chao, W.C., Murayama, Y., Muñoz, S., Costa, A., Uhlmann, F., and Singleton, M.R. (2015).
498 Structural Studies Reveal the Functional Modularity of the Scc2-Scc4 Cohesin Loader. *Cell*
499 *Rep* *12*, 719-725.
- 500 7. Hinshaw, S.M., Makrantonis, V., Kerr, A., Marston, A.L., and Harrison, S.C. (2015). Structural
501 evidence for Scc4-dependent localization of cohesin loading. *Elife* *4*, e06057.
- 502 8. Murayama, Y., and Uhlmann, F. (2014). Biochemical reconstitution of topological DNA
503 binding by the cohesin ring. *Nature* *505*, 367-371.
- 504 9. Parenti, I., Diab, F., Gil, S.R., Mulugeta, E., Casa, V., Berutti, R., Brouwer, R.W.W., Dupé, V.,
505 Eckhold, J., Graf, E., et al. (2020). MAU2 and NIPBL Variants Impair the Heterodimerization of
506 the Cohesin Loader Subunits and Cause Cornelia de Lange Syndrome. *Cell Rep* *31*, 107647.

- 507 10. Nishiyama, T., Ladurner, R., Schmitz, J., Kreidl, E., Schleiffer, A., Bhaskara, V., Bando, M.,
508 Shirahige, K., Hyman, A.A., Mechtler, K., et al. (2010). Sororin mediates sister chromatid
509 cohesion by antagonizing Wapl. *Cell* *143*, 737-749.
- 510 11. Nishiyama, T., Sykora, M.M., Huis In 't Veld, P.J., Mechtler, K., and Peters, J.M. (2013). Aurora
511 B and Cdk1 mediate Wapl activation and release of acetylated cohesin from chromosomes by
512 phosphorylating Sororin. *Proc Natl Acad Sci U S A* *110*, 13404-13409.
- 513 12. Sumara, I., Vorlaufer, E., Stukenberg, P.T., Kelm, O., Redemann, N., Nigg, E.A., and Peters,
514 J.M. (2002). The dissociation of cohesin from chromosomes in prophase is regulated by Polo-
515 like kinase. *Mol Cell* *9*, 515-525.
- 516 13. Kitajima, T.S., Sakuno, T., Ishiguro, K.I., Iemura, S.I., Natsume, T., Kawashima, S.A., and
517 Watanabe, Y. (2006). Shugoshin collaborates with protein phosphatase 2A to protect
518 cohesin. *Nature*.
- 519 14. Liu, H., Rankin, S., and Yu, H. (2013). Phosphorylation-enabled binding of SGO1-PP2A to
520 cohesin protects sororin and centromeric cohesion during mitosis. *Nat Cell Biol* *15*, 40-49.
- 521 15. Liang, C., Chen, Q., Yi, Q., Zhang, M., Yan, H., Zhang, B., Zhou, L., Zhang, Z., Qi, F., Ye, S., et al.
522 (2018). A kinase-dependent role for Haspin in antagonizing Wapl and protecting mitotic
523 centromere cohesion. *EMBO Rep* *19*, 43-56.
- 524 16. Zhou, L., Liang, C., Chen, Q., Zhang, Z., Zhang, B., Yan, H., Qi, F., Zhang, M., Yi, Q., Guan, Y., et
525 al. (2017). The N-Terminal Non-Kinase-Domain-Mediated Binding of Haspin to Pds5B Protects
526 Centromeric Cohesion in Mitosis. *Curr Biol* *27*, 992-1004.
- 527 17. London, N., and Biggins, S. (2014). Signalling dynamics in the spindle checkpoint response.
528 *Nat Rev Mol Cell Biol* *15*, 736-748.
- 529 18. Dai, J., Sullivan, B.A., and Higgins, J.M. (2006). Regulation of mitotic chromosome cohesion by
530 haspin and aurora B. *Dev Cell* *11*, 741-750.
- 531 19. Hengeveld, R.C.C., Vromans, M.J.M., Vleugel, M., Hadders, M.A., and Lens, S.M.A. (2017).
532 Inner centromere localization of the CPC maintains centromere cohesion and allows mitotic
533 checkpoint silencing. *Nat Commun* *8*, 15542.
- 534 20. Kawashima, S.A., Yamagishi, Y., Honda, T., Ishiguro, K., and Watanabe, Y. (2010).
535 Phosphorylation of H2A by Bub1 prevents chromosomal instability through localizing
536 shugoshin. *Science* *327*, 172-177.
- 537 21. Wang, F., Dai, J., Daum, J.R., Niedzialkowska, E., Banerjee, B., Stukenberg, P.T., Gorbsky, G.J.,
538 and Higgins, J.M. (2010). Histone H3 Thr-3 Phosphorylation by Haspin Positions Aurora B at
539 Centromeres in Mitosis. *Science*.
- 540 22. Yamagishi, Y., Honda, T., Tanno, Y., and Watanabe, Y. (2010). Two histone marks establish
541 the inner centromere and chromosome bi-orientation. *Science* *330*, 239-243.
- 542 23. Sullivan, B.A., and Karpen, G.H. (2004). Centromeric chromatin exhibits a histone
543 modification pattern that is distinct from both euchromatin and heterochromatin. *Nat Struct*
544 *Mol Biol* *11*, 1076-1083.
- 545 24. Kang, J., Chaudhary, J., Dong, H., Kim, S., Brautigam, C.A., and Yu, H. (2011). Mitotic
546 centromeric targeting of HP1 and its binding to Sgo1 are dispensable for sister-chromatid
547 cohesion in human cells. *Mol Biol Cell* *22*, 1181-1190.
- 548 25. Yamagishi, Y., Sakuno, T., Shimura, M., and Watanabe, Y. (2008). Heterochromatin links to
549 centromeric protection by recruiting shugoshin. *Nature*.
- 550 26. Yi, Q., Chen, Q., Liang, C., Yan, H., Zhang, Z., Xiang, X., Zhang, M., Qi, F., Zhou, L., and Wang, F.
551 (2018). HP1 links centromeric heterochromatin to centromere cohesion in mammals. *EMBO*
552 *Rep* *19*.
- 553 27. Eot-Houllier, G., Fulcrand, G., Watanabe, Y., Magnaghi-Jaulin, L., and Jaulin, C. (2008).
554 Histone deacetylase 3 is required for centromeric H3K4 deacetylation and sister chromatid
555 cohesion. *Genes Dev* *22*, 2639-2644.
- 556 28. Herz, H.M., Garruss, A., and Shilatifard, A. (2013). SET for life: biochemical activities and
557 biological functions of SET domain-containing proteins. *Trends Biochem Sci* *38*, 621-639.

- 558 29. Kumar, A., Kumari, N., Nallabelli, N., and Prasad, R. (2019). Pathogenic and Therapeutic Role
559 of H3K4 Family of Methylases and Demethylases in Cancers. *Indian J Clin Biochem* 34, 123-
560 132.
- 561 30. Han, X., Piao, L., Zhuang, Q., Yuan, X., Liu, Z., and He, X. (2018). The role of histone lysine
562 methyltransferase NSD3 in cancer. *Onco Targets Ther* 11, 3847-3852.
- 563 31. Lucio-Eterovic, A.K., and Carpenter, P.B. (2011). An open and shut case for the role of NSD
564 proteins as oncogenes. *Transcription* 2, 158-161.
- 565 32. Li, Y., Trojer, P., Xu, C.F., Cheung, P., Kuo, A., Drury, W.J., 3rd, Qiao, Q., Neubert, T.A., Xu,
566 R.M., Gozani, O., et al. (2009). The target of the NSD family of histone lysine
567 methyltransferases depends on the nature of the substrate. *J Biol Chem* 284, 34283-34295.
- 568 33. Wagner, E.J., and Carpenter, P.B. (2012). Understanding the language of Lys36 methylation
569 at histone H3. *Nat Rev Mol Cell Biol* 13, 115-126.
- 570 34. Li, W., Tian, W., Yuan, G., Deng, P., Sengupta, D., Cheng, Z., Cao, Y., Ren, J., Qin, Y., Zhou, Y.,
571 et al. (2021). Molecular basis of nucleosomal H3K36 methylation by NSD methyltransferases.
572 *Nature* 590, 498-503.
- 573 35. Rahman, S., Sowa, M.E., Ottinger, M., Smith, J.A., Shi, Y., Harper, J.W., and Howley, P.M.
574 (2011). The Brd4 extraterminal domain confers transcription activation independent of
575 pTEFb by recruiting multiple proteins, including NSD3. *Mol Cell Biol* 31, 2641-2652.
- 576 36. Yuan, G., Flores, N.M., Hausmann, S., Lofgren, S.M., Kharchenko, V., Angulo-Ibanez, M.,
577 Sengupta, D., Lu, X., Czaban, I., Azhibek, D., et al. (2021). Elevated NSD3 histone methylation
578 activity drives squamous cell lung cancer. *Nature* 590, 504-508.
- 579 37. Kim, S.M., Kee, H.J., Eom, G.H., Choe, N.W., Kim, J.Y., Kim, Y.S., Kim, S.K., Kook, H., Kook, H.,
580 and Seo, S.B. (2006). Characterization of a novel WHSC1-associated SET domain protein with
581 H3K4 and H3K27 methyltransferase activity. *Biochem Biophys Res Commun* 345, 318-323.
- 582 38. Angrand, P.O., Apiou, F., Stewart, A.F., Dutrillaux, B., Losson, R., and Chambon, P. (2001).
583 NSD3, a new SET domain-containing gene, maps to 8p12 and is amplified in human breast
584 cancer cell lines. *Genomics* 74, 79-88.
- 585 39. Bennett, R.L., Swaroop, A., Troche, C., and Licht, J.D. (2017). The Role of Nuclear Receptor-
586 Binding SET Domain Family Histone Lysine Methyltransferases in Cancer. *Cold Spring Harb*
587 *Perspect Med* 7.
- 588 40. Zhou, Z., Thomsen, R., Kahns, S., and Nielsen, A.L. (2010). The NSD3L histone
589 methyltransferase regulates cell cycle and cell invasion in breast cancer cells. *Biochem*
590 *Biophys Res Commun* 398, 565-570.
- 591 41. Vermeulen, M., Eberl, H.C., Matarese, F., Marks, H., Denissov, S., Butter, F., Lee, K.K., Olsen,
592 J.V., Hyman, A.A., Stunnenberg, H.G., et al. (2010). Quantitative interaction proteomics and
593 genome-wide profiling of epigenetic histone marks and their readers. *Cell* 142, 967-980.
- 594 42. Zentner, G.E., and Henikoff, S. (2013). Regulation of nucleosome dynamics by histone
595 modifications. *Nat Struct Mol Biol* 20, 259-266.
- 596 43. Linares-Saldana, R., Kim, W., Bolar, N.A., Zhang, H., Koch-Bojalad, B.A., Yoon, S., Shah, P.P.,
597 Karnay, A., Park, D.S., Luppino, J.M., et al. (2021). BRD4 orchestrates genome folding to
598 promote neural crest differentiation. *Nat Genet* 53, 1480-1492.
- 599 44. Shen, C., Ipsaro, J.J., Shi, J., Milazzo, J.P., Wang, E., Roe, J.S., Suzuki, Y., Pappin, D.J., Joshua-
600 Tor, L., and Vakoc, C.R. (2015). NSD3-Short Is an Adaptor Protein that Couples BRD4 to the
601 CHD8 Chromatin Remodeler. *Mol Cell* 60, 847-859.
- 602 45. Lopez-Serra, L., Kelly, G., Patel, H., Stewart, A., and Uhlmann, F. (2014). The Scc2-Scc4
603 complex acts in sister chromatid cohesion and transcriptional regulation by maintaining
604 nucleosome-free regions. *Nat Genet* 46, 1147-1151.
- 605 46. Muñoz, S., Minamino, M., Casas-Delucchi, C.S., Patel, H., and Uhlmann, F. (2019). A Role for
606 Chromatin Remodeling in Cohesin Loading onto Chromosomes. *Mol Cell* 74, 664-673 e665.
- 607 47. Muñoz, S., Passarelli, F., and Uhlmann, F. (2020). Conserved roles of chromatin remodellers
608 in cohesin loading onto chromatin. *Curr Genet* 66, 951-956.

- 609 48. Manning, B.J., and Yusufzai, T. (2017). The ATP-dependent chromatin remodeling enzymes
610 CHD6, CHD7, and CHD8 exhibit distinct nucleosome binding and remodeling activities. *J Biol*
611 *Chem* 292, 11927-11936.
- 612 49. Hakimi, M.A., Bochar, D.A., Schmiesing, J.A., Dong, Y., Barak, O.G., Speicher, D.W., Yokomori,
613 K., and Shiekhattar, R. (2002). A chromatin remodelling complex that loads cohesin onto
614 human chromosomes. *Nature* 418, 994-998.
- 615 50. Kagey, M.H., Newman, J.J., Bilodeau, S., Zhan, Y., Orlando, D.A., van Berkum, N.L., Ebmeier,
616 C.C., Goossens, J., Rahl, P.B., Levine, S.S., et al. (2010). Mediator and cohesin connect gene
617 expression and chromatin architecture. *Nature* 467, 430-435.
- 618 51. Zuin, J., Franke, V., van Ijcken, W.F., van der Sloot, A., Krantz, I.D., van der Reijden, M.I.,
619 Nakato, R., Lenhard, B., and Wendt, K.S. (2014). A cohesin-independent role for NIPBL at
620 promoters provides insights in CdLS. *PLoS Genet* 10, e1004153.
- 621 52. Kuo, A.J., Cheung, P., Chen, K., Zee, B.M., Kioi, M., Lauring, J., Xi, Y., Park, B.H., Shi, X., Garcia,
622 B.A., et al. (2011). NSD2 links dimethylation of histone H3 at lysine 36 to oncogenic
623 programming. *Mol Cell* 44, 609-620.
- 624 53. Zhu, L., Li, Q., Wong, S.H., Huang, M., Klein, B.J., Shen, J., Ikenouye, L., Onishi, M.,
625 Schneidawind, D., Buechele, C., et al. (2016). ASH1L Links Histone H3 Lysine 36 Dimethylation
626 to MLL Leukemia. *Cancer Discov* 6, 770-783.
- 627 54. Sumara, I., Vorlaufer, E., Gieffers, C., Peters, B.H., and Peters, J.M. (2000). Characterization of
628 vertebrate cohesin complexes and their regulation in prophase. *J Cell Biol* 151, 749-762.
- 629 55. Watrin, E., and Legagneux, V. (2005). Contribution of hCAP-D2, a non-SMC subunit of
630 condensin I, to chromosome and chromosomal protein dynamics during mitosis. *Mol Cell Biol*
631 25, 740-750.
- 632 56. Kitajima, T.S., Hauf, S., Ohsugi, M., Yamamoto, T., and Watanabe, Y. (2005). Human Bub1
633 defines the persistent cohesion site along the mitotic chromosome by affecting Shugoshin
634 localization. *Curr Biol* 15, 353-359.
- 635 57. Schmitz, J., Watrin, E., Lenart, P., Mechtler, K., and Peters, J.M. (2007). Sororin Is Required for
636 Stable Binding of Cohesin to Chromatin and for Sister Chromatid Cohesion in Interphase. *Curr*
637 *Biol*.

638

639 **Figure legends**

640 **Figure 1: NSD3 prevents premature sister chromatids separation in mitosis.** (A)
641 Representative images of chromosome spreads with magnified chromosome from HeLa cells
642 transfected for 72h with control or different SET domain methyltransferase siRNA. (B) Western
643 blotting analysis of NSD3 depletion after 72h siRNA transfection. RAD21 and α -Tubulin were
644 used as nuclear and cytoplasmic loading marker, respectively. Table indicates targeted exons
645 by respective siRNA. Note the presence of a non-specific band just below the short NSD3s
646 isoform band. (C) For each siRNA tested, cells displaying sister chromatid separation were
647 scored. 300-500 prometaphase cells were counted in each experiment and the mean and SD of
648 relative amount of prometaphase cells with cohesion defects for 5 experiments is represented.

649

650 **Figure 2: NSD3 contribution to cohesion maintenance occurs before mitotic entry.** (A-B)
651 Immunofluorescence with BUB1 (A) and SGO1 (B) antibodies after 72h NSD3 siRNA
652 treatment. CREST serum were used to label centromere position. Scale bars correspond to 10
653 μ m. (C-E) Measurement of inter-centromeres distance on chromosome 11 following NSD3 and

654 RAD 21 depletion. After 8h siRNA transfection, cells have been subjected to a double
655 thymidine-block, followed by a 6h release to enrich in G2 cells. Then, whole-cell extracts were
656 prepared for western blot to check for protein extinction (C) or FISH were performed on cells
657 with a specific probe for centromeric chromosome 11 alpha-satellite sequence (D-E). (D)
658 Representative images of FISH experiments with 4X magnified view of one the three
659 chromosome 11 centromere loci. (E) Box plot representation of the distance between paired
660 FISH signals. (n= 162 for each tested siRNA from three independent experiments, 5-95
661 percentiles are indicated).

662

663 **Figure 3: NSD3 depletion reduces cohesin and kollerin loading at mitotic exit.**

664 Synchronized control or NSD3-depleted cells were arrested in mitosis by nocodazole treatment.
665 Mitotic cells were collected by shake-off and released from the arrest. At the indicated time
666 points, chromatin-bound fractions were prepared and analyzed by western-blot. Topoisomerase
667 II was used as a control for chromatin-associated proteins. p-H3S10 and CAP-D2 were analyzed
668 to monitor progression through mitosis. Histones were stained with Coomassie to show the
669 equivalence of protein amount between lanes. Representative capture of western-blot are shown
670 on the left part of the panel. Quantification of signal intensity of the corresponding images are
671 represented on the right part of the panel in black or red for cells treated with Luc or NSD3
672 siRNA, respectively.

673

674 **Figure 4: NSD3 localization during the cell cycle.** Proliferative HeLa cells were fixed

675 immediately (A) or after a 1 min 0.1% triton incubation to extract the cell soluble content (B).
676 (C) Representative images of interphasic or mitotic cells transfected for 72h with Luc or NSD3
677 siRNA. Cells were swollen by hypotonic treatment and spotted on a slide by cyto-centrifugation
678 before immuno-labelling with NSD3 and CREST serum. (D) and (E): Representative images
679 from metaphase to telophase of LAP-NSD3L expressing cells immuno-labelled with RAD21
680 (D) or MAU2 (E). For all image panels, scale bars correspond to 10 μ m.

681

682 **Figure 5: Depletion of NSD3 long isoform induces premature separation of sister**

683 **chromatids.** (A) Western-blot analysis of specific NSD3 isoforms depletion efficiency after
684 72h transfection with the indicated siRNA. RAD21 and actin were used as nuclear and cellular
685 loading marker, respectively. Note that, at the long exposure time used to ensure that NSD3s is
686 properly depleted, the NSD3s band and the non-specific band observed just below appear to be
687 fused in Luc, NSD3L-A and NSD3L-B lanes. (B) Percentage of prometaphase with separated
688 sister chromatids in cells depleted for specific NSD3 isoforms. Data represents mean and SD
689 of three independent experiments. 150-300 prometaphase cells were counted for each condition
690 in individual experiments. (C) Representative images of the nuclear presence of inducible LAP-
691 NSD3 after doxycyclin induction in the LAP-NSD3L HeLa cell line. Scale bar correspond to

692 20 μ m. (D) Western-blot analysis of the various exogenous and endogenous form of NSD3
693 following endogenous NSD3 depletion and concomitant LAP-NSD3L induction in the LAP-
694 NSD3L HeLa cell line. LAP-tag fused with NSD3L generates a heavier band than NSD3L
695 which is detected only following doxycyclin induction. α -Tubulin and MAU2 were used as
696 cytoplasmic and nuclear loading marker, respectively. (E) Representative images of a
697 microscope field with cells expressing (1) or not (2) LAP-NSD3L after 72h doxycyclin
698 induction and immuno-labelling with anti-GFP antibodies to improve signal detection. The left
699 panel shows GFP labelling merged with CREST serum and DNA signals. 9X magnification of
700 a representative paired centromeric region were shown for each indicated mitotic cell. On the
701 right panel, the percentage of prometaphases displaying separated sister chromatids is shown
702 following 72h siRNA depletion. Data is displayed according to doxycyclin induction and the
703 presence or the absence of GFP labeling in the doxycyclin induced LAP-NSD3L HeLa cells.
704 Data represents mean and SD of three independent experiments. 100-300 prometaphase cells
705 were counted for each condition in individual experiments.

706

707

708 **Supplemental figure legends**

709 **Figure S1: Screening for contribution of SET domain methyltransferases to prevent sister**
710 **chromatid separation in mitosis.** For each of the 14 evaluated methyltransferases, 3 different
711 siRNA were tested. Cells were transfected for 72h before fixation and chromosome spreading.
712 300-500 prometaphase cells were counted and the proportion of mitotic cells with separated
713 chromatids was assessed according to the phenotypes shown in figure 1A.

714

715 **Figure S2: NSD3 depletion does not affect cohesin and MAU2 expression level or global**
716 **di-methylation level of H3K4 and H3K36.** Synchronized control or NSD3-depleted cells were
717 arrested in mitosis by nocodazole treatment as indicated in the figure. Mitotic cells were then
718 collected by shake-off and released from the arrest. At the indicated time points, whole-cell
719 extracts were prepared and analyzed by western-blot. α -Tubulin and Histone H4 were used as
720 cytoplasmic and nuclear loading marker, respectively. Decrease in p-H3S10 signal indicated
721 the efficiency of nocodazole release.

722

723 **Figure S3: Efficiency of NSD3 depletion shown by immunofluorescence.** HeLa cells were
724 transfected with the indicated siRNA for 48h and soluble cell content was pre-extracted before
725 immunofluorescence. Scale bar corresponds to 10 μ m.

726

727 **Figure S4: Cellular localization of LAP-NSD3L during the cell cycle.** Proliferative LAP-
728 NSD3L HeLa cell line was fixed immediately (left panel) or after a 1 min 0.1% triton incubation
729 to extract cell soluble content (right panel). Cells were immuno-labeled for p-H3S10 to identify

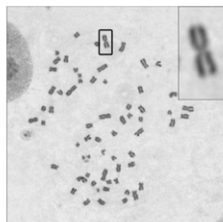
730 precisely the different mitotic phases. Representative images are shown and scale bar
731 correspond to 10 μm .

732

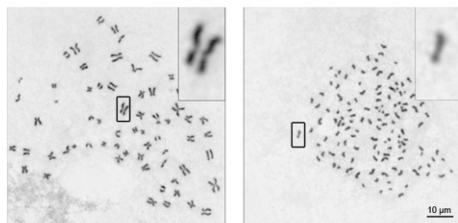
733 **Figure S5: Timing of LAP-NSD3L, MAU2 and RAD21 recruitment onto chromatin**
734 **following metaphase-anaphase transition.** Representative images from metaphase to
735 telophase of LAP-NSD3L expressing cells that were pre-extracted before immunolabelling
736 with RAD21 (A) or MAU2 (B) as indicated in the material and methods section a. For all
737 image panels, scale bars correspond to 10 μm .

A

Normal cohesion

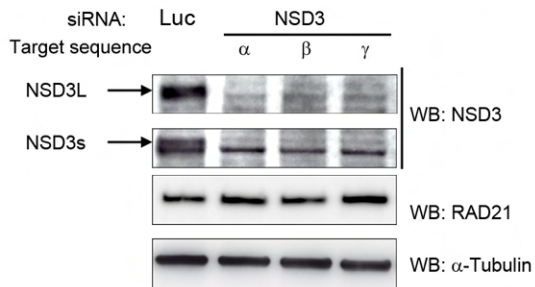


cohesion defects



B

siRNA	siRNA NSD3- α	siRNA NSD3- β	siRNA NSD3- γ
Targeted exon	5	6	2



C

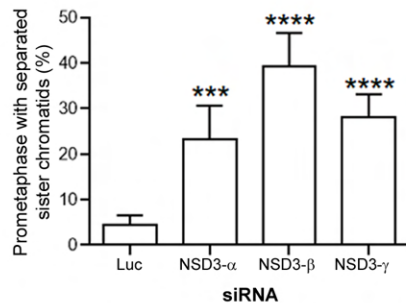


Figure 1: NSD3 prevents premature sister chromatids separation in mitosis

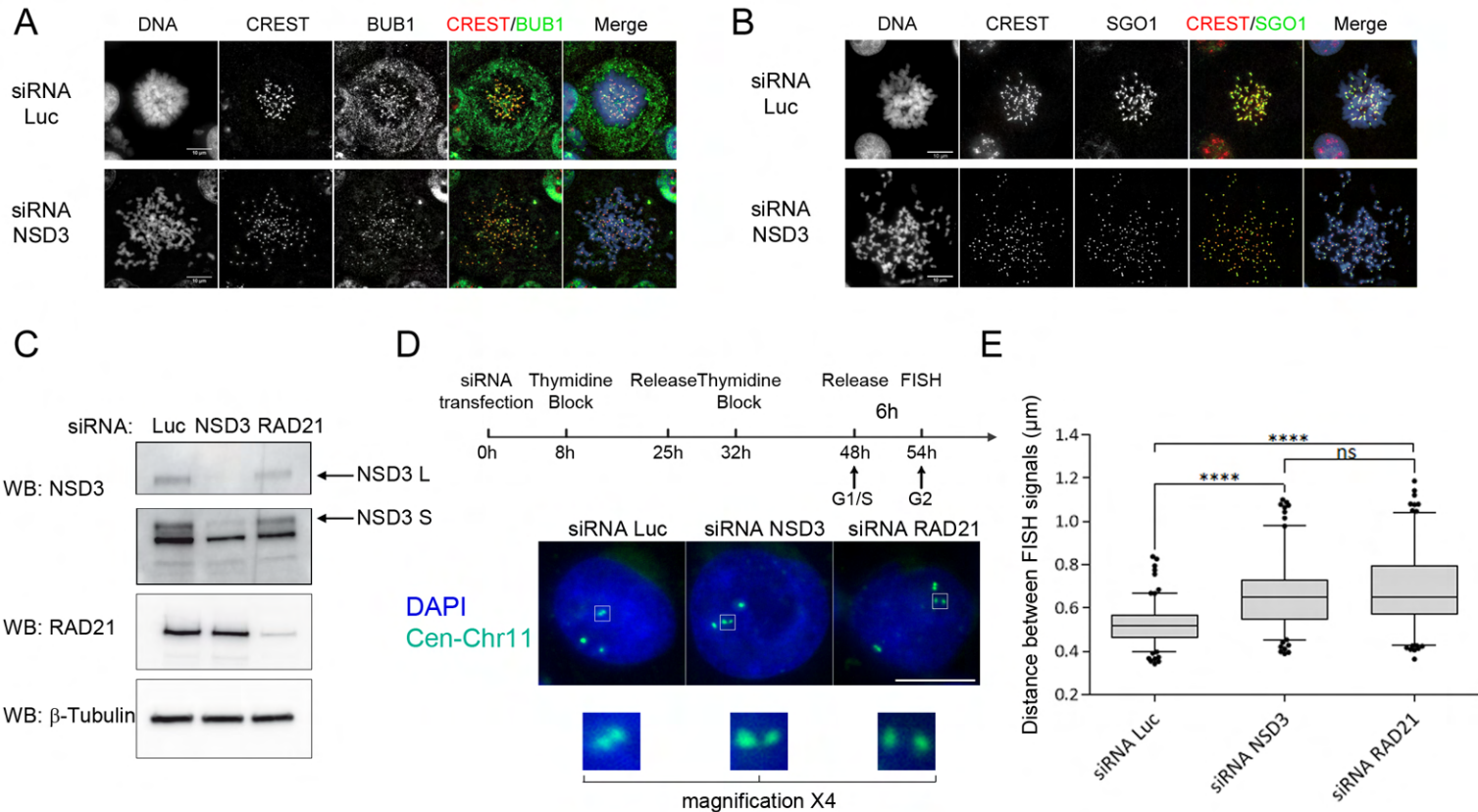


Figure 2: NSD3 contribution to cohesion maintenance occurs before mitotic entry

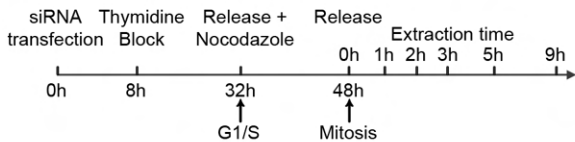
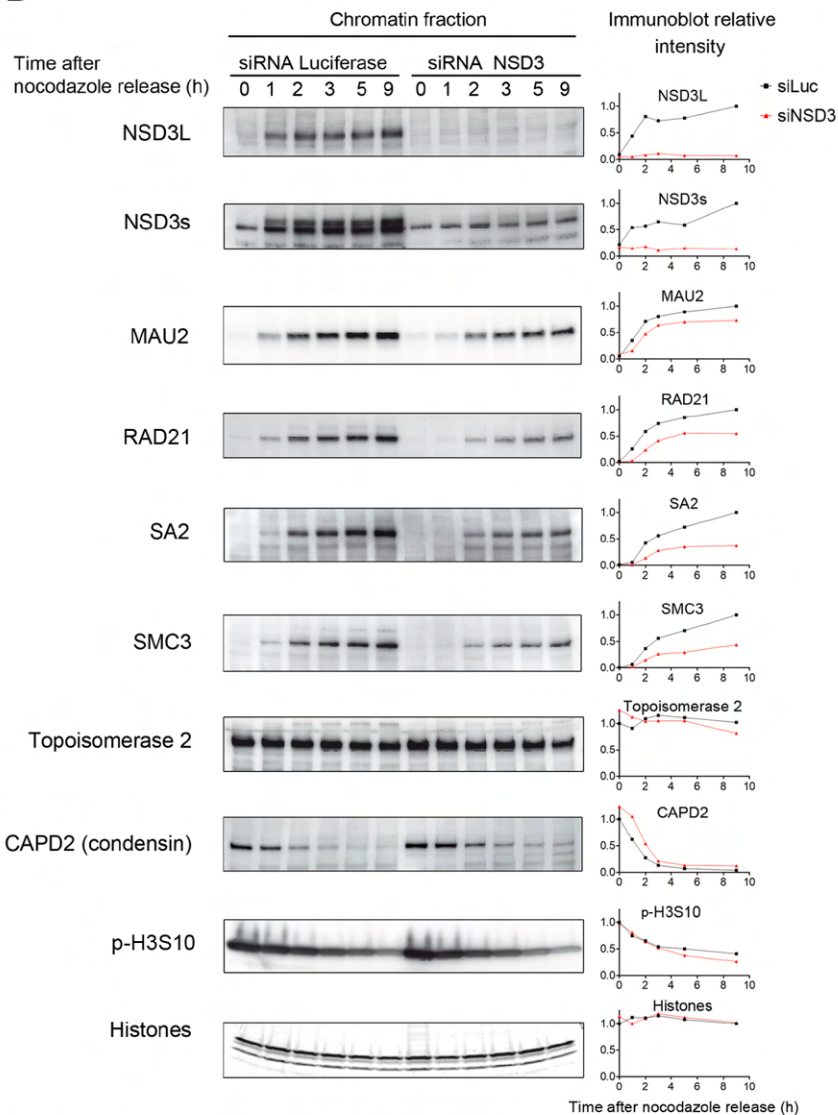
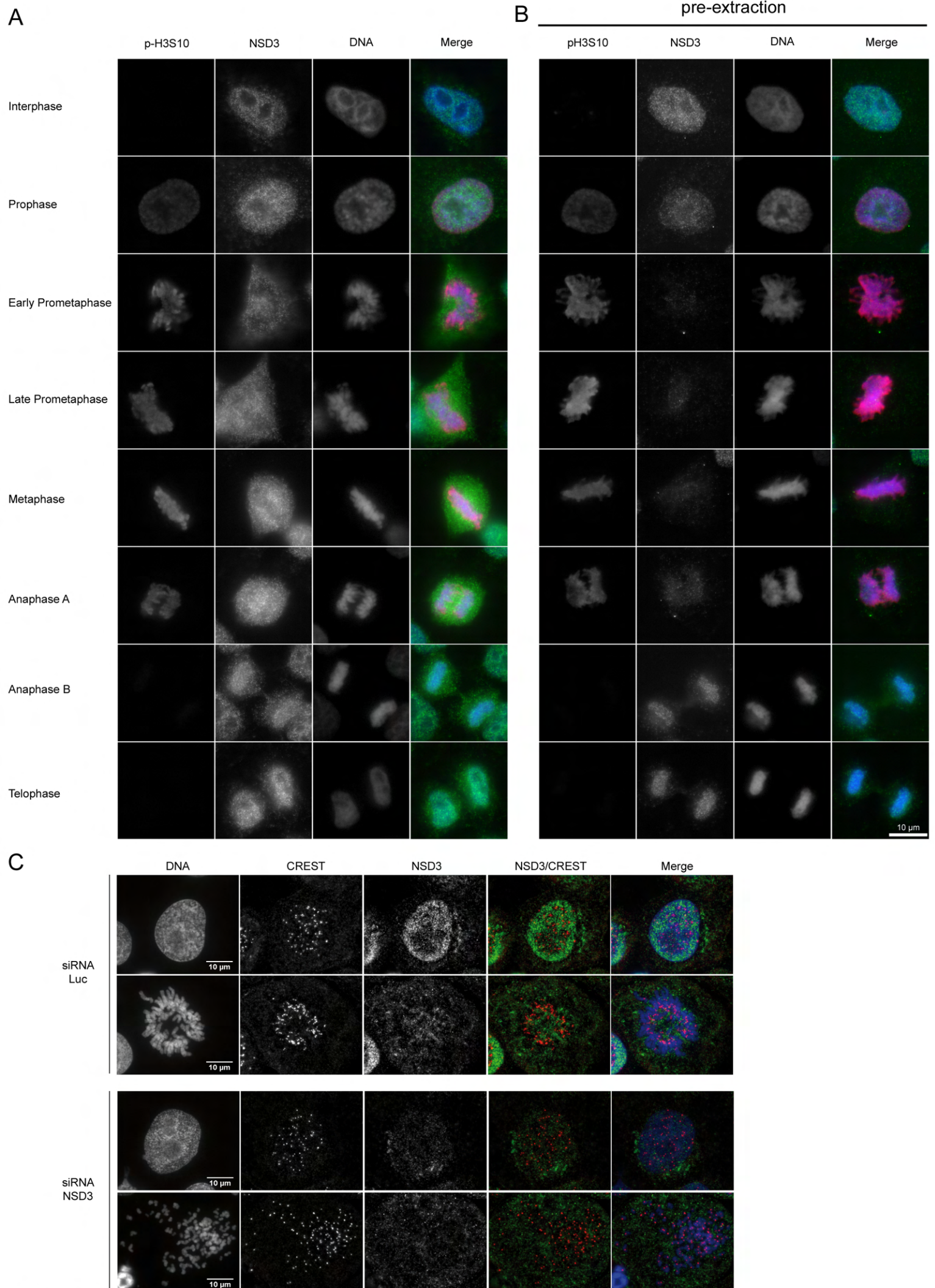
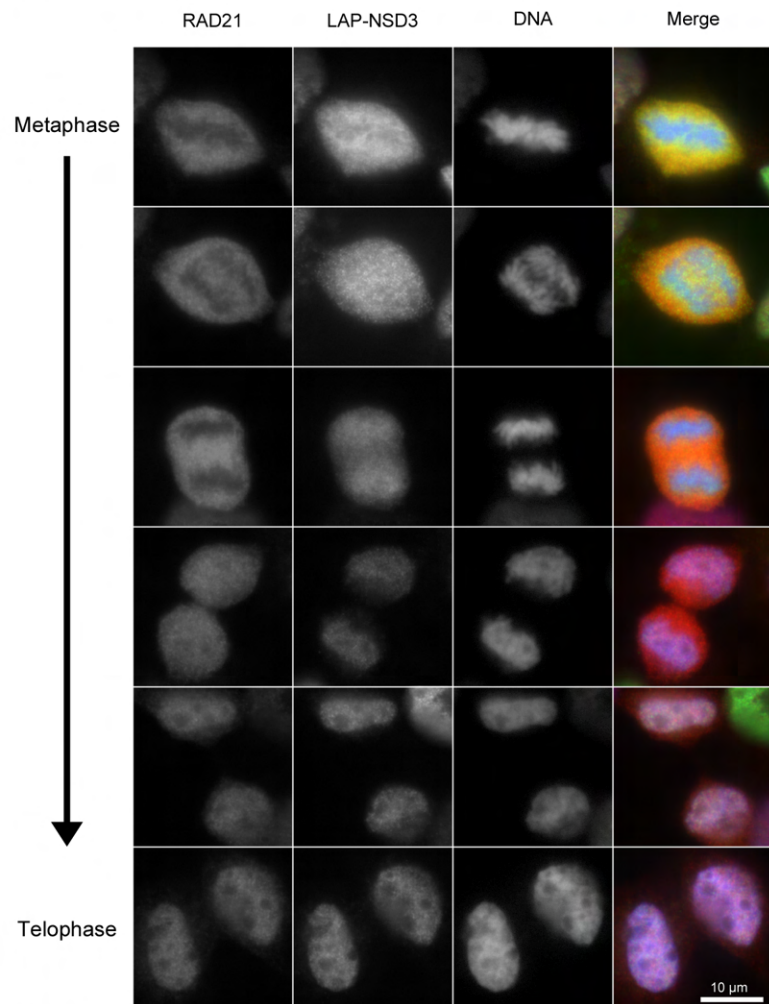
A**B**

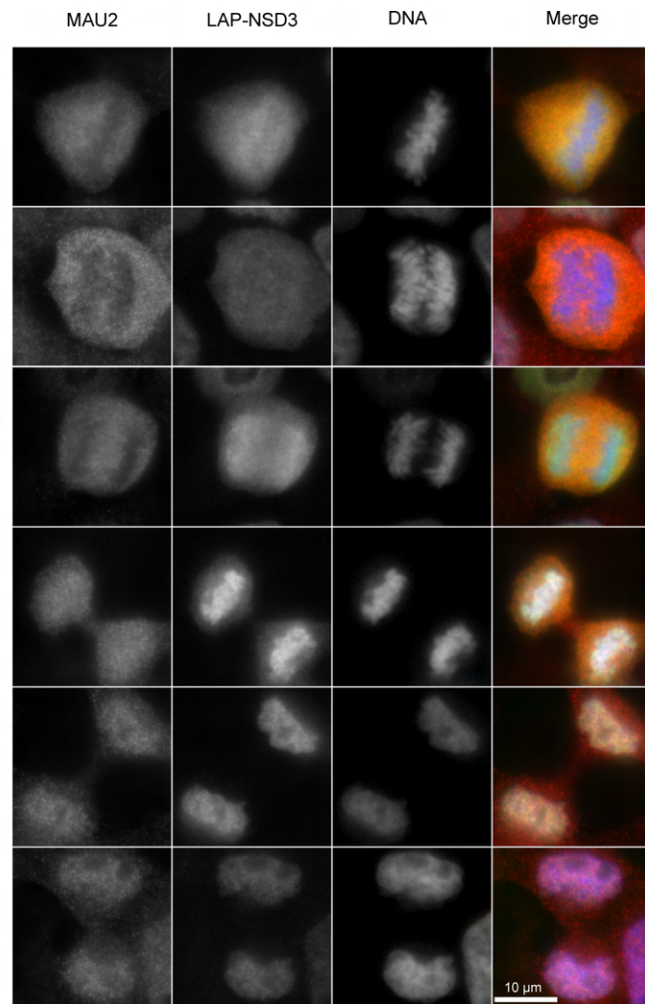
Figure 3: NSD3 depletion reduces cohesin and kollerin loading at mitotic exit



D



E



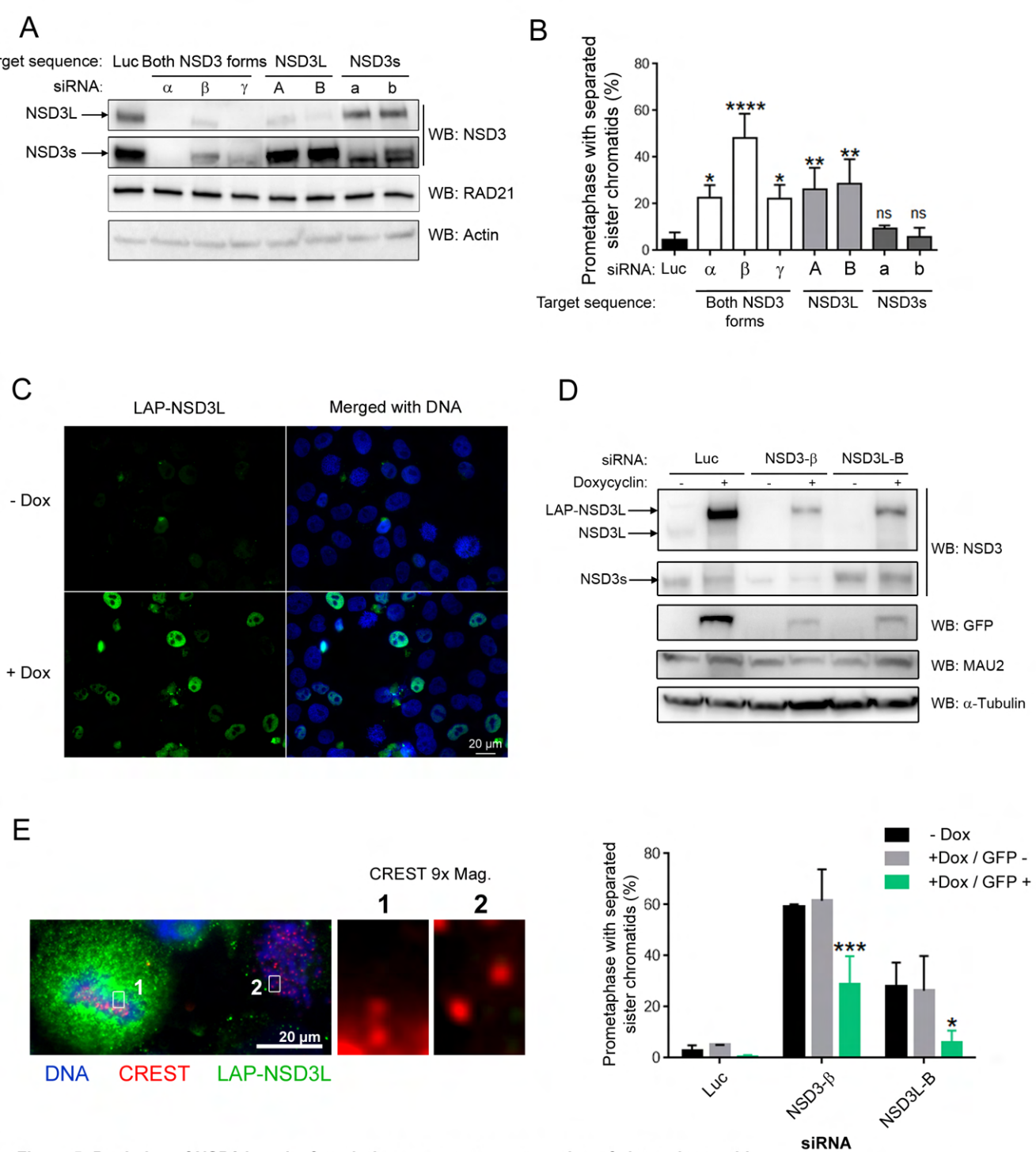
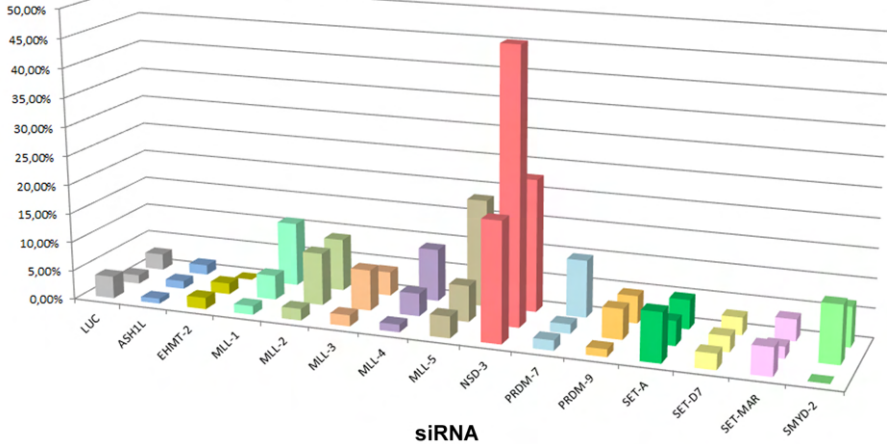


Figure 5: Depletion of NSD3 long isoform induces premature separation of sister chromatids

Prometaphase with separated sister chromatids (%)



siRNA

Figure S1: Screening for contribution of SET domain methyltransferases to prevent sister chromatid separation in mitosis

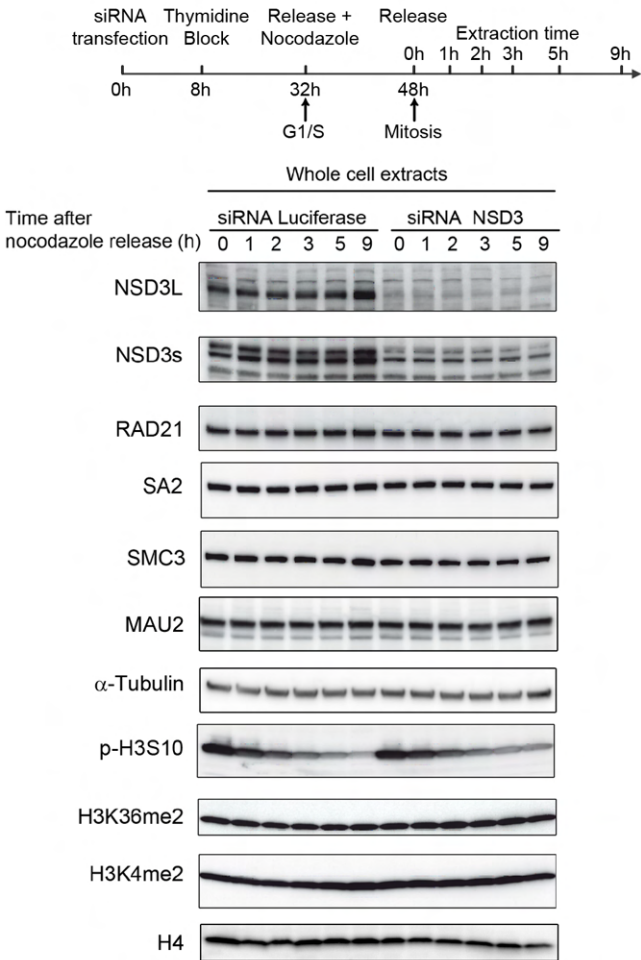


Figure S2: NSD3 depletion does not affect cohesin and MAU2 expression level or global di-methylation level of H3K4 and H3K36

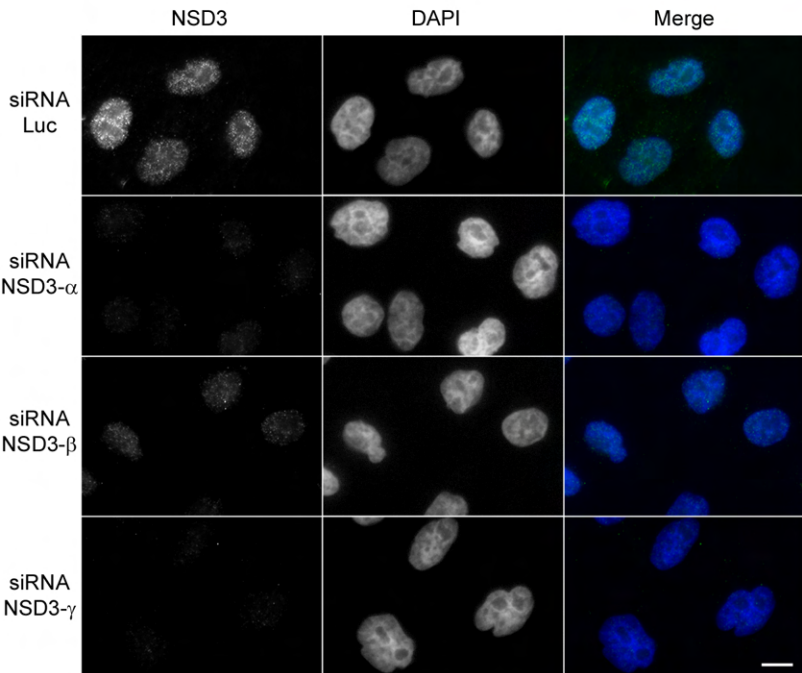


Figure S3: Efficiency of NSD3 depletion shown by immunofluorescence

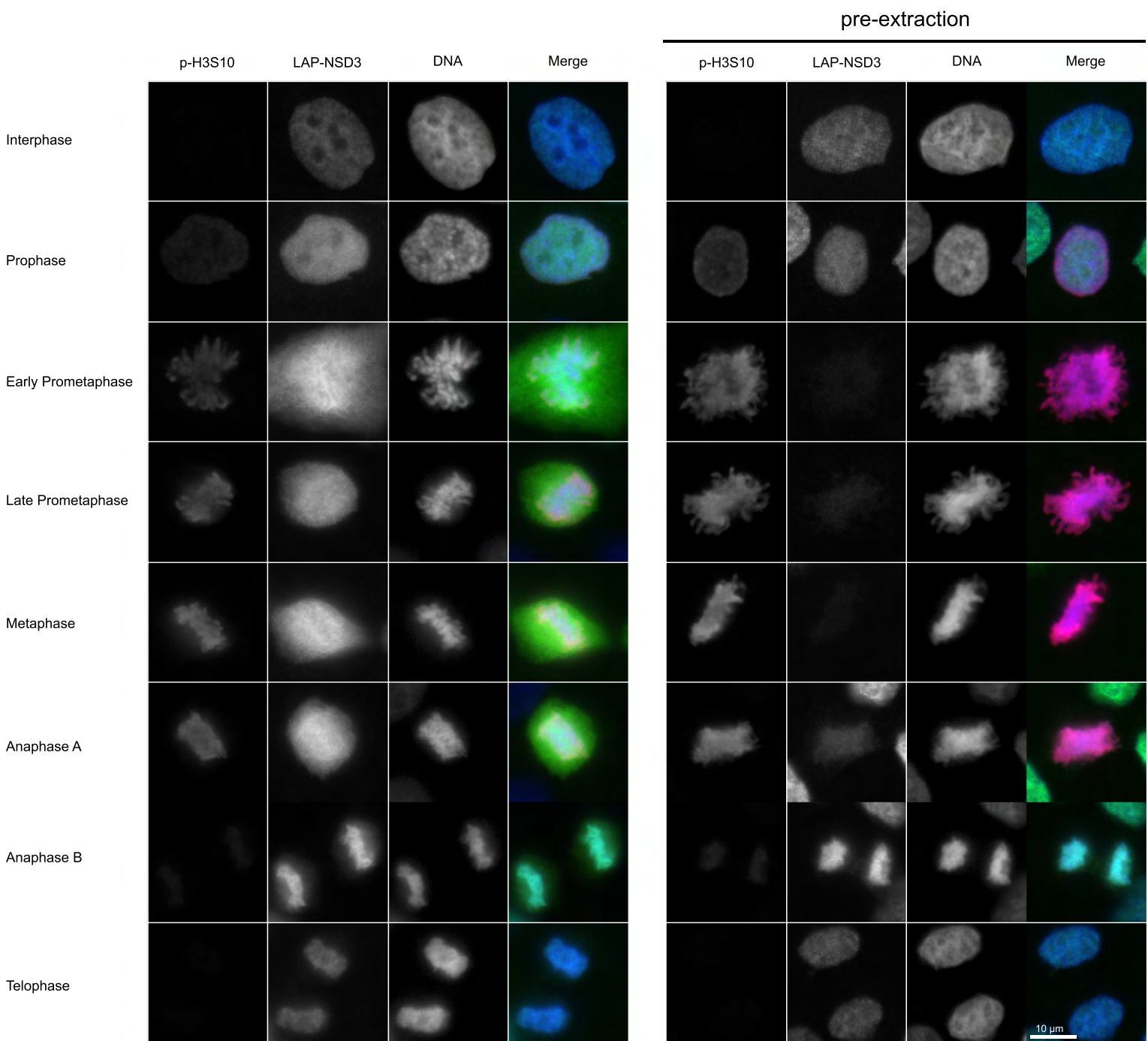
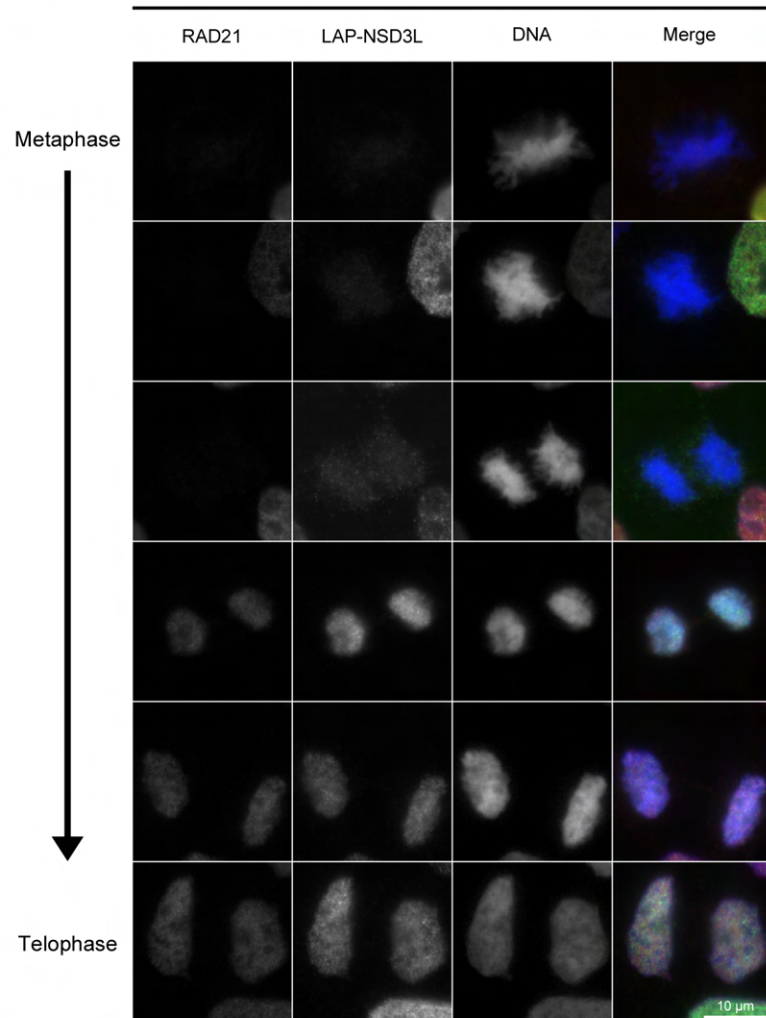


Figure S4: Cellular localization of LAP-NSD3L during the cell cycle

A

pre-extraction



B

pre-extraction

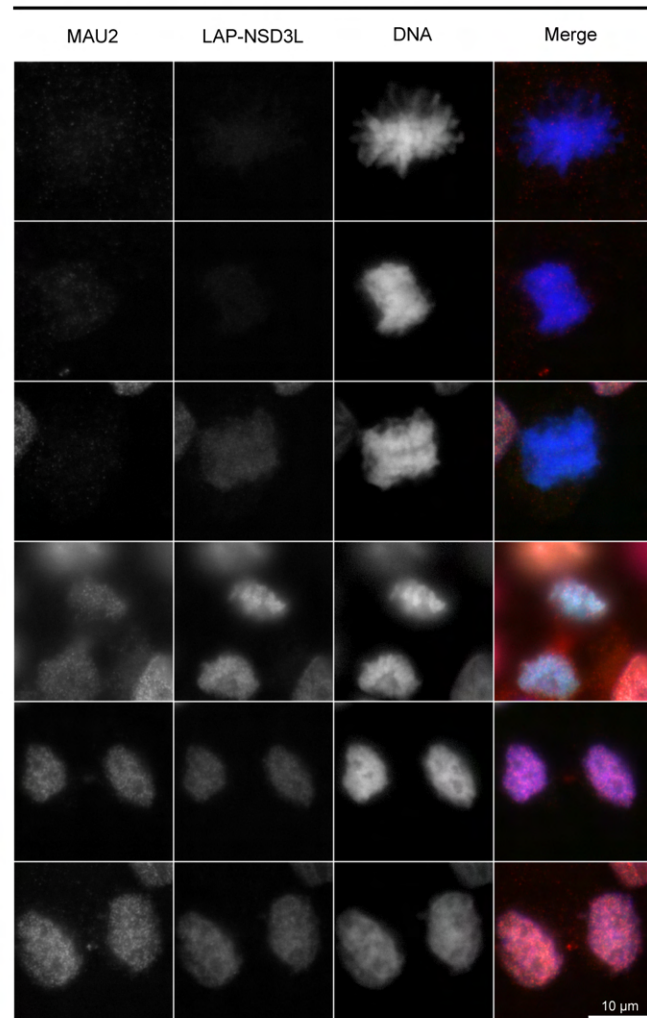


Figure S5: Timing of LAP-NSD3L, MAU2 and RAD21 recruitment onto chromatin following metaphase-anaphase transition